Ground-Based Remote Sensing Cloud Detection Using Dual Pyramid Network and Encoder–Decoder Constraint

Zhong Zhang, *Senior Member, IEEE*, Shuzhen Yang, Shuang Liu, *Senior Member, IEEE*, Xiaozhong Cao, and Tariq S. Durrani, *Life Fellow, IEEE*

***Abstract*— Many methods for ground-based remote sensing cloud detection learn representation features using the encoder–decoder structure. However, they only consider the information from single scale, which leads to incomplete feature extraction. In this article, we propose a novel deep network named dual pyramid network (DPNet) for ground-based remote sensing cloud detection, which possesses an encoder–decoder structure with dual pyramid pooling module (DPPM). Specifically, we process the feature maps of different scales in the encoder through dual pyramid pooling. Then, we fuse the outputs of the dual pyramid pooling in the same pyramid level using the attention fusion. Furthermore, we propose the encoder–decoder constraint (EDC) to relieve information loss in the process of encoding and decoding. It constrains the values and the gradients of probability maps from the encoder and the decoder to be consistent. Since the number of cloud images in the publicly available databases for ground-based remote sensing cloud detection is limited, we release the TJNU Large-scale Cloud Detection Database (TLCDD) that is the largest database in this field. We conduct a series of experiments on TLCDD, and the experimental results verify the effectiveness of the proposed method.**

***Index Terms*— Dual pyramid pooling module (DPPM), encoder–decoder constraint (EDC), ground-based remote sensing cloud detection.**

I. Introduction

CLOUD is an important weather phenomenon, and it has a great influence on the Earth's radiation budget and climate change [1], [2]. Hence, cloud observation has drawn a lot of attention from both academia and industry due to its wide applications in weather forecasting and military operations [3], [4]. Cloud observation is mainly classified into the satellite cloud observation and the ground-based cloud observation [5]–[7]. The satellite cloud observation is more suitable for describing large-scale cloud information and changes, while the ground-based cloud observation is good at reflecting local cloud information [8]–[11]. In addition, the ground-based cloud observation has many advantages, such as low equipment cost, simple operation, and easy acquisition of data. The ground-based cloud observation mainly contains three tasks, i.e., cloud shape, cloud cover, and cloud base height [12]. In this article, we focus on ground-based remote sensing cloud detection, which is the key technology for cloud cover estimation. There are two reasons for the urgent need to develop an automatic ground-based remote sensing cloud detection algorithm. First, the detection results marked by different weather observers may be inconsistent due to their different skill levels. Second, manually labeling cloud images for ground-based remote sensing cloud detection is labor-intensive and tedious because this process is pixel-level labeled. When the ground-based cloud data are huge, the labeling process is very difficult.

Hence, many methods for ground-based remote sensing cloud detection have been proposed, and they are roughly divided into three categories, namely, threshold-based methods, texture-based methods, and deep learning methods. Some threshold-based methods directly treat R and B values as the threshold to distinguish cloud and sky or employ adaptive thresholds, e.g., Ostu algorithm and superpixel segmentation [13], [14]. The texture-based methods utilize the texture features to describe the local regions of cloud images [15], [16]. However, the performance of threshold-based methods and texture-based methods is unsatisfactory because these methods are not learning-based, which is easily affected by the environmental changes.

Recently, convolutional neural network (CNN) achieves extraordinary performance in many fields, such as image recognition, speech analysis, and object detection because of its deep network structure and changeable perception field [14], [17], [18]. CNN is also introduced in the field of remote sensing cloud detection, and many researchers [14], [18], [19] design the deep network as a structure with the

Manuscript received September 27, 2021; revised December 25, 2021 and March 12, 2022; accepted March 28, 2022. Date of publication March 31, 2022; date of current version April 19, 2022. This work was supported in part by the National Natural Science Foundation of China under Grant 62171321, in part by the Natural Science Foundation of Tianjin under Grant 20JCZDJC00180 and Grant 19JCZDJC31500, in part by the Open Projects Program of National Laboratory of Pattern Recognition under Grant 202000002, and in part by the Tianjin Higher Education Creative Team Funds Program. *(Corresponding author: Shuang Liu.)*

Zhong Zhang, Shuzhen Yang, and Shuang Liu are with the Tianjin Key Laboratory of Wireless Mobile Communications and Power Transmission, Tianjin Normal University, Tianjin 300387, China (e-mail: zhong.zhang8848@gmail.com; ysz2020zhen@gmail.com; shuangliu.tjnu@gmail.com).

Xiaozhong Cao is with the Meteorological Observation Centre, China Meteorological Administration, Beijing 100081, China (e-mail: xzhongcao@163.com).

Tariq S. Durrani is with the Department of Electronic and Electrical Engineering, University of Strathclyde, Glasgow G1 1XQ, U.K. (e-mail: t.durrani@strath.ac.uk).

Digital Object Identifier 10.1109/TGRS.2022.3163917

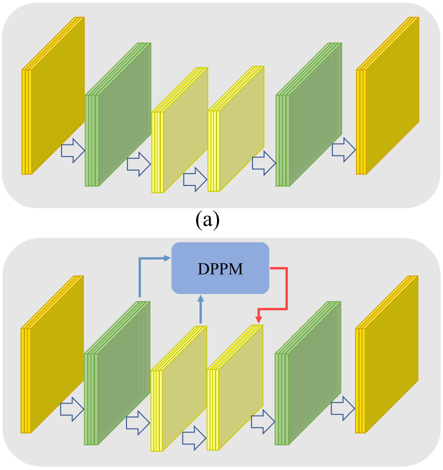
(a)

(b)

Fig. 1. Structures of (a) common-used deep network and (b) DPNet for ground-based remote sensing cloud detection.

encoder and the decoder, as shown in Fig. 1(a). However, there are two limitations for these methods. First, in the encoding process, they only consider the information from one scale, which leads to incomplete feature extraction. Second, the feature maps are conducted by max-pooling operations in the encoding process, which results in information loss. Meanwhile, the convolution operations have a negative impact on edge detail information.

To overcome the first limitation, we propose a novel deep network named dual pyramid network (DPNet) for ground-based remote sensing cloud detection, which possesses an encoder–decoder structure with dual pyramid pooling module (DPPM), as shown in Fig. 1(b). The proposed DPPM combines the information from different scales of the encoder via fusing dual pyramids. Specifically, we process the feature maps of different scales in the encoder via spatial pyramid pooling. Then, we fuse the feature maps in the same pyramid level from different scales by learning attention weights that reflect the importance of different elements in the feature maps. As a result, we obtain completed features.

Furthermore, we propose the encoder–decoder constraint (EDC) to relieve information loss. The quality of probability maps directly determines the performance of cloud detection, and meanwhile, the information communication between the encoder and the decoder could fully utilize the information of them. Hence, the proposed EDC constrains the probability maps from the encoder and the decoder. In order to reflect the detail information and the local boundary, EDC expects the values and the gradients of probability maps from the encoder and the decoder to be consistent, simultaneously.

A large-scale database is necessary for the development of ground-based remote sensing cloud detection algorithms, especially for deep learning-based algorithms [20]. The large-scale database could avoid model overfitting and improve the generalization ability of deep model. However, the publicly available databases on ground-based remote sensing cloud detection contain insufficient cloud images, which is difficult to meet actual demand. For example, Singapore All Weather Segmentation (SWIMSEG) database [21], CloudSegmentation database [13], Whole Sky Image SEGmentation (WSISEG) database [22], and BENCHMARK database [23] have 1013, 100, 400, and 32 cloud images, respectively. In this article, we release the TJNU Large-scale Cloud Detection Database (TLCDD) consisting of 5000 cloud images. To the best of our knowledge, TLCDD is the largest database for ground-based remote sensing cloud detection.

The contributions of this article are summarized in three aspects. First, we propose DPNet to construct dual pyramids in the encoder in order to fuse the information from different scales. Second, we propose EDC to constrain the feature maps of the encoder and the decoder so as to relieve information loss. Finally, we release the largest cloud detection database, i.e., TLCDD, and the proposed method achieves better performance than other state-of-the-art methods on TLCDD.

II. Related Work

A. Ground-Based Remote Sensing Cloud Detection

At present, more and more researchers are devoted to the ground-based remote sensing cloud detection. These studies are mainly composed of threshold-based methods, texture-based methods, and deep learning methods. The threshold-based methods usually adopt RGB color values as criteria to distinguish cloud and sky. For example, Long *et al.* [2] and Kreuter *et al.* [24] proposed to utilize the thresholds of 0.6 and 0.77 on R/B for cloud detection. When the ratio is over 0.6 or 0.77, the pixel is identified as cloud. Souzaecher *et al.* [25] recommended to employ B-R for identifying cloud, and the pixels with B-R > 30 are classified as sky. The above methods directly utilize the fixed threshold to detect cloud and easily affected by environmental changes. To overcome the drawback, some researchers present adaptive threshold algorithms. Yang *et al.* [26] calculated the adaptive threshold based on the B-R feature image using the Otsu algorithm. The superpixel segmentation algorithm [13], [27] was utilized to divide the cloud image into a series of subregions and further detect cloud in each subregion. Furthermore, texture feature extraction as a better kind of methods is used in cloud detection. For example, Başeski and Cenaras [15] applied the homogenous texture descriptor (HTD) as the complement of color features for cloud detection. The HTD could describe the regularity, directionality, and coarseness of texture. Tulpan *et al.* [16] proposed to utilize six kinds of image moments for cloud detection, where the image moments include the area of the image, two edge detectors, a cross detector, and the elongation and direction of the image. The threshold-based methods and the texture-based methods solve the difficulty of manually labeling cloud pixels to a certain extent, but the performance is unsatisfactory. Thus, the ground-based remote sensing cloud detection algorithms still need to be improved.

CNN possesses the strong capability of feature representation, so it has been widely used in many research fields with excellent performance [17], [19], [28], [29]. Inspired by this, many researchers design different network structures under the framework of CNN to improve the performance of ground-based remote sensing cloud detection. For example,

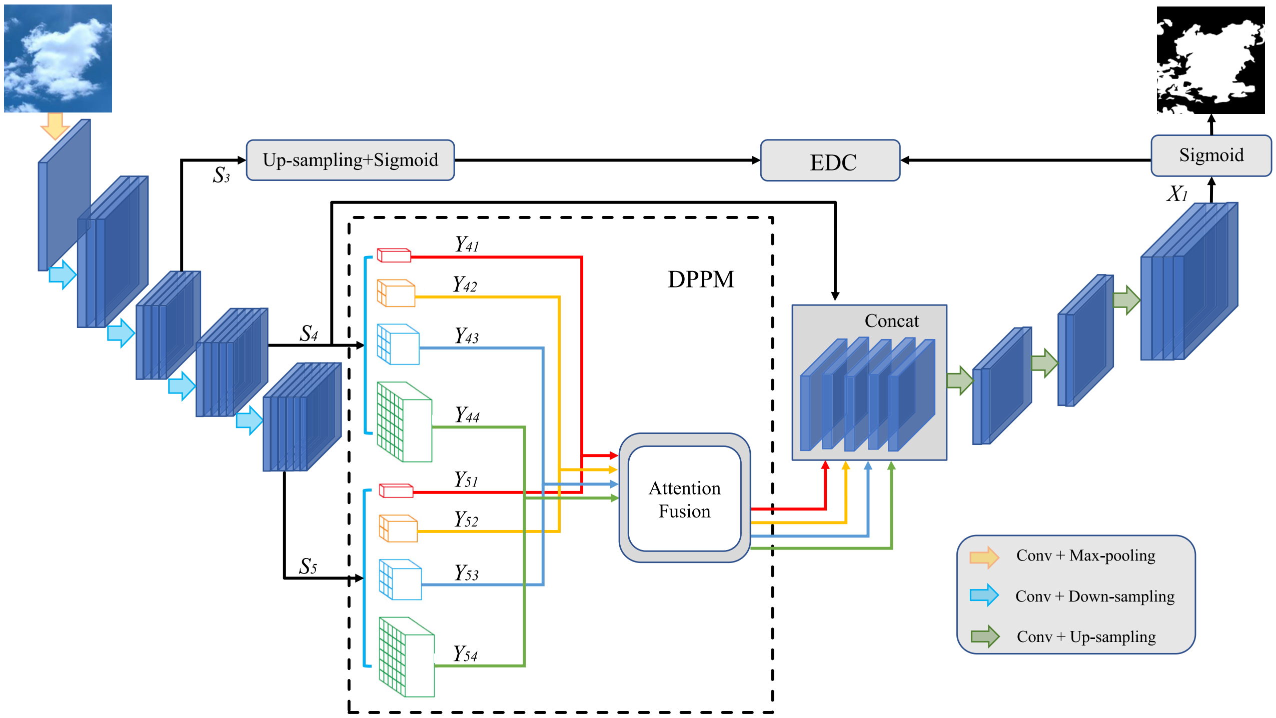

Fig. 2. Framework of DPNet. S_3, S_4, and S_5 are the feature maps from Scale3, Scale4, and Scale5, respectively, Y_{4i} and Y_{5i} are the outputs of pyramid pooling, and X_1 is the feature maps of the decoder.

Dev *et al.* [18] proposed the CloudSegNet where the basic structure is designed as the encoder–decoder structure. In the training stage, CloudSegNet is optimized by daytime and nighttime cloud images. Xie *et al.* [14] presented the SegCloud model, which possesses a symmetric encoder–decoder structure followed by a softmax classifier. The softmax classifier realizes the pixel classification and outputs the segmentation results. Zhang *et al.* [30] proposed the multiscale attention convolutional neural network (MACNN) for cloud detection by exploiting multiscale information and attention connection between the encoder and the decoder.

B. Encoder–Decoder Structure for Semantic Segmentation

The task of cloud detection is to classify each pixel of cloud image into cloud or sky, which is regarded as a two-category segmentation problem. Hence, we introduce semantic segmentation [31]–[34] in this section. The encoder–decoder structure, which mainly includes an encoder and a decoder, dominates the semantic segmentation task [18]. The encoder maps an image to a specific high-dimensional feature to capture semantic information. The decoder gradually transforms the high-dimensional feature into the score map for the sequence segmentation, and it restores object detail and spatial information. The high-dimensional feature is treated as the bridge between the original image and the score map. Furthermore, the skip connection is usually inserted into the encoder–decoder structure, and it realizes the feature fusion between the encoder and the decoder [35], which is beneficial to preserve the detail information from the encoder [23], [36].

Long *et al.* [37] presented the fully convolutional network (FCN) for semantic segmentation, which could accept the image with any size. It utilizes the deconvolution layer to upsample the feature maps in the last layer in order to restore to the size of input image. The widely used U-Net [23] is a typical encoder–decoder network, in which the encoder contains convolution and max-pooling operations and the decoder restores the feature maps to the original resolution through convolution and upsampling operations. Some methods [28], [34], [38] presented the spatial pyramid structure under the framework of the encoder–decoder structure to aggregate the context information based on different regions. However, most existing encoder–decoder methods extract incomplete features in the encoding processing, and meanwhile, they suffer from the information loss in the encoding and decoding process. Therefore, we propose DPNet and EDC to overcome these limitations.

III. Approach

In this section, we first present an overview of the proposed DPNet, as shown in Fig. 2. We then describe the major parts of DPNet, i.e., encoder–decoder structure and DPPM. Finally, we introduce how to implement EDC.

A. Overview of DPNet

1) Encoder–Decoder Structure: We apply the encoder–decoder structure to conduct the pixel labeling in the cloud image. The encoder is designed as the common used ResNet-50 [39], which utilizes the max-pooling operations and the convolution operations to continuously reduce the size of feature maps and increase the number of channels. The decoder employs the upsampling operations to increase the size of feature maps continuously.

TABLE I
STRUCTURE OF ENCODER

Name	Input Size	Filters	Output Size
Scale1	512×512	$\begin{bmatrix}3\times3,64,s=2\\3\times3,64,s=1\\3\times3,128,s=1\end{bmatrix}\times1$	256×256
Max-pooling	256×256	$3\times3,\ s=2$	128×128
Scale2	128×128	$\begin{bmatrix}1\times1,64,s=1\\3\times3,64,s=1\\1\times1,256,s=1\end{bmatrix}\times3$	128×128
Scale3	128×128	$\begin{bmatrix}1\times1,128,s=1\\3\times3,128,s=1\\1\times1,512,s=1\end{bmatrix}\times4$	128×128
Scale4	64×64	$\begin{bmatrix}1\times1,256,s=1\\3\times3,256,s=1\\1\times1,1024,s=1\end{bmatrix}\times6$	64×64
Scale5	64×64	$\begin{bmatrix}1\times1,512,s=1\\3\times3,512,s=1\\1\times1,2048,s=1\end{bmatrix}\times3$	64×64

TABLE II
STRUCTURE OF DECODER

Name	Input Size	Filters	Output Size
Up-sampling	64×64	$2\times2,\ s=2$	128×128
Conv	128×128	$\begin{bmatrix}3\times3,1024,s=1\end{bmatrix}\times2$	128×128
Up-sampling	128×128	$2\times2,\ s=2$	256×256
Conv	256×256	$\begin{bmatrix}3\times3,256,s=1\end{bmatrix}\times2$	256×256
Up-sampling	256×256	$2\times2,\ s=2$	512×512
Conv	512×512	$\begin{bmatrix}3\times3,64,s=1\\3\times3,64,s=1\\3\times3,16,s=1\\3\times3,1,s=1\end{bmatrix}$	512×512

2) Dual Pyramid Pooling Module: The proposed DPPM aims to extract completed information from cloud images during the encoding process. The feature maps from two scales are conducted by the pyramid pooling to obtain different pyramid levels. Afterward, we apply attention mechanism to fuse the feature maps from different scales under the same pyramid level. In this way, each pixel is assigned to different attention weight, which is beneficial to the subsequent decoding process.

3) Encoder–Decoder Constraint: The information loss occurs in the process of encoding and decoding, and therefore, we exchange the information between them to overcome this drawback. The proposed EDC contains two constraints that expect the probability maps from the encoder and the decoder to be consistent in different aspects.

B. Encoder–Decoder Structure

The proposed DPNet utilizes an asymmetric encoder–decoder structure. The encoder consists of five scales, and each scale contains several blocks. The detailed information of the encoder is listed in Table I. Here, s represents the size of stride. Scale2–Scale5 include three, four, six, and three blocks, respectively, and each block contains three convolutional layers. Taking Scale5 as an example, it contains three blocks where each block consists of three convolutional layers with the sizes of 1 × 1, 3 × 3, and 1 × 1, and the numbers of filters are 512, 512, and 2048, respectively.

The decoder is composed of three upsampling layers and three convolutional blocks, and the structure is shown in Table II. After each upsampling layer, the size of feature maps is doubled, and the decoder outputs the feature maps that have the same size of the input image.

C. Dual Pyramid Pooling Module

The pyramid pooling [40] is usually inserted into the segmentation networks, such as PSPNet to exploit contextual information by pooling feature maps at different pyramid levels. The pyramid pooling is formulated as

$$Y_i = P(S, k_i), \quad i = 1, 2, 3, 4 \tag{1}$$

where P refers to the average pooling, S represents the feature maps, and k_i indicates the ith pyramid level. Normally, there are four pyramid levels ($i = 1, 2, 3,$ and 4), and the bin sizes of four pyramid levels are 1 × 1, 2 × 2, 3 × 3, and 6 × 6, respectively. However, the pyramid pooling only considers the feature maps from one scale and ignores the information from different scales. Hence, we propose the dual pyramid pooling, which conducts the pyramid pooling on the feature maps from different scales and fuse them via the attention fusion. It is formulated as

$$Z_i = A(P(S_4, k_i), P(S_5, k_i)), \quad i = 1, 2, 3, 4 \tag{2}$$

where S_4 and S_5 are the feature maps from Scale4 and Scale5, respectively, and A indicates the attention fusion.

From (2), we can see that the feature maps from different scales should be fused together. Some segmentation networks, such as U-Net [23] and FCN [37], are usually direct addition or concatenation to fuse the feature maps. They treat all elements in the feature maps equally and ignore the importance of different elements. Hence, we propose the attention fusion to assign different weights to the elements in order to fuse the feature maps from different scales after pyramid pooling. The attention fusion is formulated as

$$A(Y_{4i}, Y_{5i}) = W_i Y_{4i} + Y_{5i} \tag{3}$$

where W_i is the attention coefficient of the ith pyramid level.

Fig. 3 shows the flowchart of attention fusion, where the feature maps Y_{4i} and Y_{5i} are the outputs of pyramid pooling from Scale4 and Scale5, respectively. Y_{4i} and Y_{5i} are processed

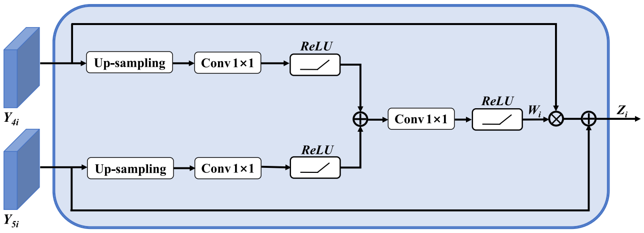

Fig. 3. Flowchart of the attention fusion.

by the upsampling operation, the convolutional layer with the kernel size of 1 × 1, and the rectified linear unit (ReLU) activation. Afterward, the obtained feature maps are added in the elementwise manner and then fed into the convolutional layer with the kernel size of 1 × 1 and the ReLU activation to obtain the attention coefficient W_i.

D. Encoder–Decoder Constraint

The encoder–decoder structure dominates the field of cloud detection, but this structure easily causes the information loss due to the following two reasons. First, the max pooling in the encoder reduces the size of feature maps, which results in the information loss. Second, the convolutional layers have a negative impact on edge detail information. Furthermore, after a series of convolutional layers, it is hard to find the corresponding position in the cloud image.

In order to solve the abovementioned issues, we propose EDC to constrain the probability maps, which consists of two constraint terms. The first constraint term of EDC focuses on constraining the probability maps from the encoder and the decoder. Specifically, the feature maps S_3 in the encoder are fed into the upsampling layer and the sigmoid function, and then, we obtain the probability map S_3', which is the same size as the input image. The feature maps X_1 in the decoder are input into the sigmoid function to obtain the probability map X_1'. Then, this constraint expects that the probability maps from the encoder and the decoder are consistent

$$L_1 = \frac{1}{H \times W}\left\| S_3' - X_1' \right\|_1 \tag{4}$$

where H and W are the height and the width of the probability maps, respectively, and $\|\cdot\|_1$ is the l_1 norm of matrix.

The edge information is vital to the ground-based remote sensing cloud detection, and therefore, the second term of EDC utilizes the gradients of probability maps of the encoder and the decoder. It is formulated as

$$L_2 = \frac{1}{H \times W}\left\| G\left(S_3'\right) - G\left(X_1'\right) \right\|_2 \tag{5}$$

where $\|\cdot\|_2$ is the l_2 norm of matrix and G is the Prewitt operator [41], which is utilized to compute the gradient. G consists of two templates G_x and G_y, where G_x detects horizontal edges and G_y detects vertical edges. They are defined as

$$G_x = \begin{pmatrix} 1, & 0, & -1 \\ 1, & 0, & -1 \\ 1, & 0, & -1 \end{pmatrix} \tag{6}$$

$$G_y = \begin{pmatrix} 1, & 1, & 1 \\ 0, & 0, & 0 \\ -1, & -1, & -1 \end{pmatrix}. \tag{7}$$

The expressions of the probability maps S_3' and X_1' after going through G are

$$G\left(S_3'\right) = G_x * S_3' + G_y * S_3' \tag{8}$$

$$G\left(X_1'\right) = G_x * X_1' + G_y * X_1' \tag{9}$$

where $*$ represents the convolution operation.

The loss of EDC is expressed as

$$L_E = L_1 + \alpha L_2 \tag{10}$$

where α is the parameter to balance the two constraints.

Furthermore, we apply the binary cross-entropy loss after the probability map X_1' to optimize the network

$$L_G = -\frac{1}{H \times W}\sum_{i=1}^{H \times W} y_i \ln x_i + (1 - y_i)\ln(1 - x_i) \tag{11}$$

where y_i is the ground-truth label and x_i is the element value of X_1'. In a word, the total loss of the proposed method is formulated as

$$L = L_G + \beta L_E \tag{12}$$

where β is the parameter to balance the importance of different components.

IV. Experiments

In this section, we evaluate the performance of the proposed method on TLCDD. We first introduce the TLCDD and the implementation details of our experiments. Afterward, we show the experimental results to verify the superiority of the proposed method.

A. TJNU Large-Scale Cloud Detection Database

The TLCDD, which consists of 5000 cloud images, is utilized to study the ground-based remote sensing cloud detection. There are 4208 images for training and 792 images for testing. It has no cloud image overlap between the training set and the test set. Each cloud image in the database corresponds to a ground-truth cloud mask, which is jointly annotated by meteorologists and cloud-related researchers. The cloud image is stored in the PNG format with a pixel resolution of 512 × 512. The collection of all the images in the database lasted for two years and came from nine provinces of China, including Tianjin, Anhui, Sichuan, Gansu, Shandong, Hebei, Liaoning, Jiangsu, and Hainan. As a result, the TLCDD guarantees the diversity of cloud images, which makes the experimental results convincing. Fig. 4 shows the cloud images and the corresponding ground-truth cloud masks.

B. Implementation Details and Evaluation Criteria

Before feeding the cloud images into the deep model, we conduct the preprocessing operations. Specifically, the cloud images are normalized by the mean values and the standard deviation values. The horizontal flip is conducted with the probability of 0.5. The size of images is 512 × 512. The

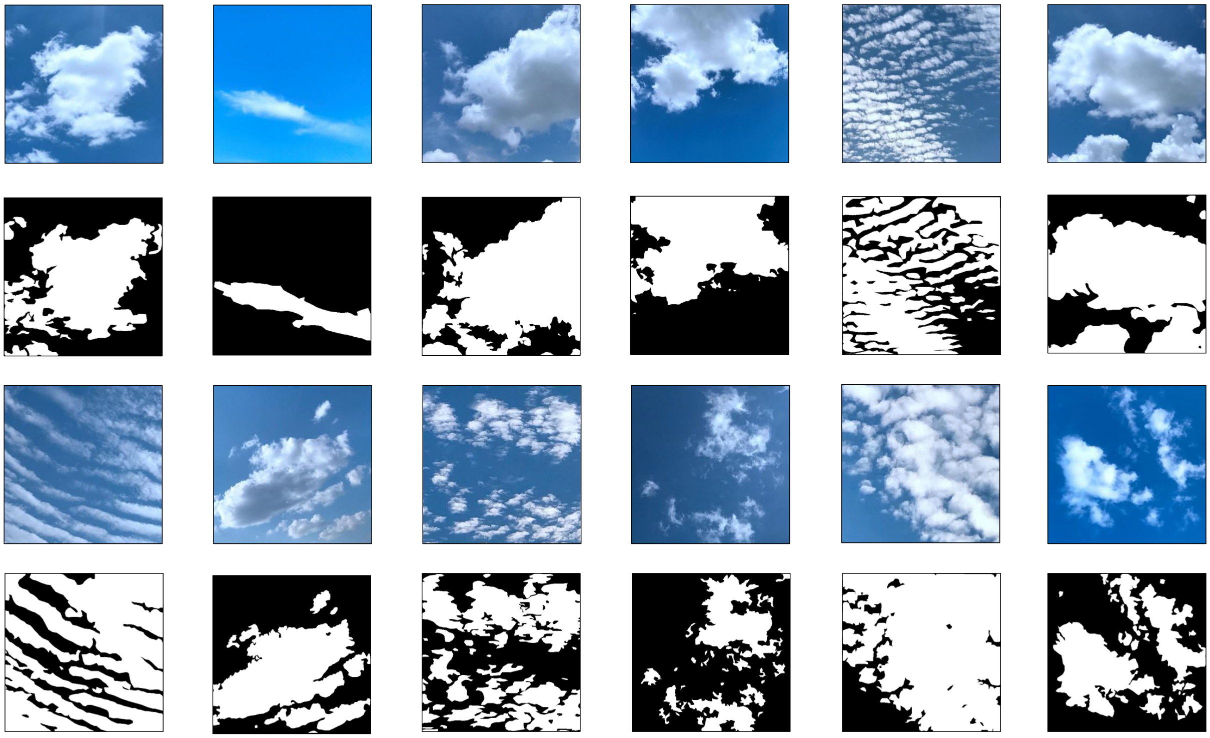

Fig. 4. Several cloud samples in TLCDD.

encoder of DPNet is initialized by the pretrained ResNet-50. Specifically, Scale2–Scale5 correspond to conv2x–conv5x in the ResNet-50 model, respectively. The proposed deep network is optimized by the stochastic gradient descent (SGD) algorithm with the weight decay of 10^{-9} and the momentum of 0.9. In the training phase, the initial learning rate is set to 0.001, and the number of training epochs is set to 45. In addition, the hyperparameter α in (10) is equal to 1.1, and β in (12) is equal to 0.4.

In order to verify the effectiveness of the proposed method, five quantitative evaluation criteria, i.e., precision (Pre), recall (Rec), F-score (F-s), accuracy (Acc), and intersection over union (IoU), are applied. The precision refers to the pixels that are correctly predicted as the cloud accounting for the pixels that are predicted as the cloud in the image. The recall refers to the proportion of pixels correctly predicted as cloud to all ground-truth cloud pixels in the image. The F-score considers both recall and precision, and it is interpreted as the harmonic mean of precision and recall. The accuracy refers to the proportion of pixels that are correctly predicted as cloud and sky to all pixels in the image. We also consider IoU in the evaluation criteria for the cloud detection task. It quantifies a ratio of overlap between the intersection and the union of two sets. The two sets indicate the set of predicted cloud pixels and the set of ground-truth cloud pixels. The ratio can also be interpreted as the number of true positives over the sum of true positives, false positives, and false negatives. In a word, the five evaluation criteria are defined as

$$\mathrm{Pre} = \frac{\mathrm{TP}}{\mathrm{TP}+\mathrm{FP}} \tag{13}$$

$$\mathrm{Rec} = \frac{\mathrm{TP}}{\mathrm{TP}+\mathrm{FN}} \tag{14}$$

$$\text{F-s} = \frac{2\times\mathrm{Pre}\times\mathrm{Rec}}{(\mathrm{Pre}+\mathrm{Rec})} \tag{15}$$

$$\mathrm{Acc} = \frac{\mathrm{TP}+\mathrm{TN}}{\mathrm{TP}+\mathrm{TN}+\mathrm{FP}+\mathrm{FN}} \tag{16}$$

$$\mathrm{IoU} = \frac{\mathrm{TP}}{\mathrm{TP}+\mathrm{FP}+\mathrm{FN}} \tag{17}$$

where TP, FP, TN, and FN denote true positives, false positives, true negatives, and false negatives, respectively.

C. Experimental Results

1) Ablation Studies: The advantage of the proposed DPNet is to learn rich and accurate features for cloud detection. We conduct ablation studies to verify the role of different components in DPNet, namely, DPPM and EDC.

Framework1 only utilizes the encoder–decoder structure to detect clouds, that is, it does not apply DPPM and EDC.

Framework2 employs the encoder–decoder structure with one pyramid pooling to extract the information from one scale. This structure is similar to PSPNet.

Framework3 applies dual pyramid pooling to extract the features from different scales and directly concatenate them without the attention fusion.

Framework4 uses the proposed DPPM to learn the features in the encoder, where the proposed DPPM contains the dual pyramid pooling and the attention fusion.

Framework5 conducts the cloud detection using the encoder–decoder structure with the first constraint term of EDC.

Framework6 inserts the second constraint term of EDC into the encoder–decoder network.

TABLE III

COMPARISONS WITH DIFFERENT ABLATION METHODS

Methods	Pre (%)	Rec (%)	F-s (%)	Acc (%)	IoU (%)
$Framework1$	67.21	76.24	66.21	76.83	56.82
$Framework2$	68.35	78.19	67.46	78.61	57.27
$Framework3$	69.18	79.93	69.09	79.57	59.82
$Framework4$	70.12	81.07	71.12	81.43	62.07
$Framework5$	69.18	80.13	71.05	79.81	60.37
$Framework6$	69.02	79.07	70.12	79.43	60.66
$Framework7$	70.16	80.33	71.77	80.20	62.47
Ours	**72.09**	**82.18**	**72.96**	**85.70**	**64.38**

TABLE IV

RESULTS OF THE INFLUENCE OF PREPROCESSING. "WITH PRE" AND "WITHOUT PRE" INDICATE THE CLOUD IMAGE WITH PREPROCESSING AND WITHOUT PROCESSING, RESPECTIVELY

Methods	Pre (%)	Rec (%)	F-s (%)	Acc (%)	IoU (%)	Time (Hours)
$With\,Pre$	**72.09**	**82.18**	**72.96**	**85.70**	**64.38**	**18.84**
$Without\,Pre$	71.34	81.65	71.64	84.21	63.98	20.46

TABLE V

EVALUATION RESULTS OF DIFFERENT METHODS ON TCLDD

Methods	Pre (%)	Rec (%)	F-s (%)	Acc (%)	IoU (%)
R/B (0.77) ([24])	65.88	22.55	25.54	69.11	18.95
B-R (30) ([25])	50.08	13.75	15.08	66.41	11.49
Otsu (B-R) ([26])	57.91	61.47	50.80	66.92	38.34
FCN ([37])	63.20	73.77	57.00	66.49	46.75
CloudSegNet ([18])	64.46	77.61	57.79	64.59	47.78
U-Net ([23])	68.80	80.43	67.32	74.13	58.16
SegCloud ([14])	68.35	80.50	66.95	73.06	57.76
PSPNet ([26])	68.74	77.75	67.00	78.64	57.43
Ours	**72.09**	**82.18**	**72.96**	**85.70**	**64.38**

Framework7 employs the proposed EDC to constrain the encoder and the decoder.

The results of ablation studies are listed in Table III from which we can draw four conclusions. First, our method achieves the best results because we combine the encoder–decoder structure with DPPM and EDC. Second, the performance of Framework2 and Framework3 is better than that of Framework1, which demonstrates that the pyramid pooling strategy is effective to the cloud detection task. Meanwhile, the performance of Framework3 is better than that of Framework2 because the dual pyramid pooling could extract the features from different scales, while the pyramid pooling learns features only from one scale. As a result, the dual pyramid pooling obtains richer and more complete information, which is beneficial to ground-based remote sensing cloud detection. Third, Framework4 obtains better results than Framework3 due to the attention fusion, which assigns different weights to the elements of feature maps.

Finally, Framework5 and Framework6 are obtained by adding the first and second constraints of EDC on the basis of Framework1, respectively. They obtain better performance than Framework1, which verifies the effectiveness of the constraints between the encoder and the decoder. Furthermore, the results of Framework7 are superior to Framework5 and Framework6, which proves that the combination of the two constraints, i.e., EDC has a further performance improvement. Furthermore, we also study the influence of cloud image preprocessing. The experimental results are listed in Table IV where we can see that the results with preprocessing are better than without preprocessing.

2) Comparisons With State-of-the-Art Methods: We compare the proposed method with other methods and the results of the evaluation criteria are listed in Table V. These compared methods contain threshold-based methods and deep learning methods. The threshold-based methods usually include R/B (0.77) [24], B-R (30) [25], and Otsu [26]. The first two methods belong to the fixed threshold algorithms that perform different operations on the R channel and B channel. Otsu is an adaptive threshold algorithm, which performs the segmentation task on the grayscale image, such as B-R by maximizing the interclass variance.

We also compare the proposed method with the deep learning methods, for example, FCN [37], U-Net [23], CloudSegNet [18], and SegCloud [14]. FCN is the first network with fully convolutional layers for pixelwise prediction. It utilizes five downsampling blocks to extract the feature maps and three deconvolution layers to restore the feature maps. It defines the skip architecture to combine deep-semantic information and shallow-appearance information. U-Net is a symmetrical encoder–decoder network, which has four max-pooling blocks and four upsampling blocks. It also utilizes the skip architecture on each corresponding convolutional block. CloudSegNet is composed of the encoder, including three convolutional layers and three max-pooling layers, and the decoder, including four deconvolution layers and three upsampling layers. SegCloud consists of ten convolutional layers and five max-pooling layers in the encoder, and five upsampling layers and ten convolutional layers in the decoder. Then, the outputs of decoder are fed into a softmax classifier.

From Table V, we can draw the following conclusions. First, the proposed method achieves the best results. Specifically, it outperforms the second highest results by 3.29%, 1.68%, 5.64%, 7.06%, and 6.22% in Pre, Rec, F-s, Acc, and IoU, respectively. Second, the adaptive threshold method achieves better performance than the fixed threshold methods because the adaptive threshold could vary with different cloud images. Third, the detection results of the deep learning methods are better than those of the threshold-based methods. It is because the deep learning methods automatically learn features from cloud images through multiple layers. Meanwhile, the threshold-based methods directly apply the thresholds on the cloud images without feature learning, which is difficult to adapt to the environmental changes.

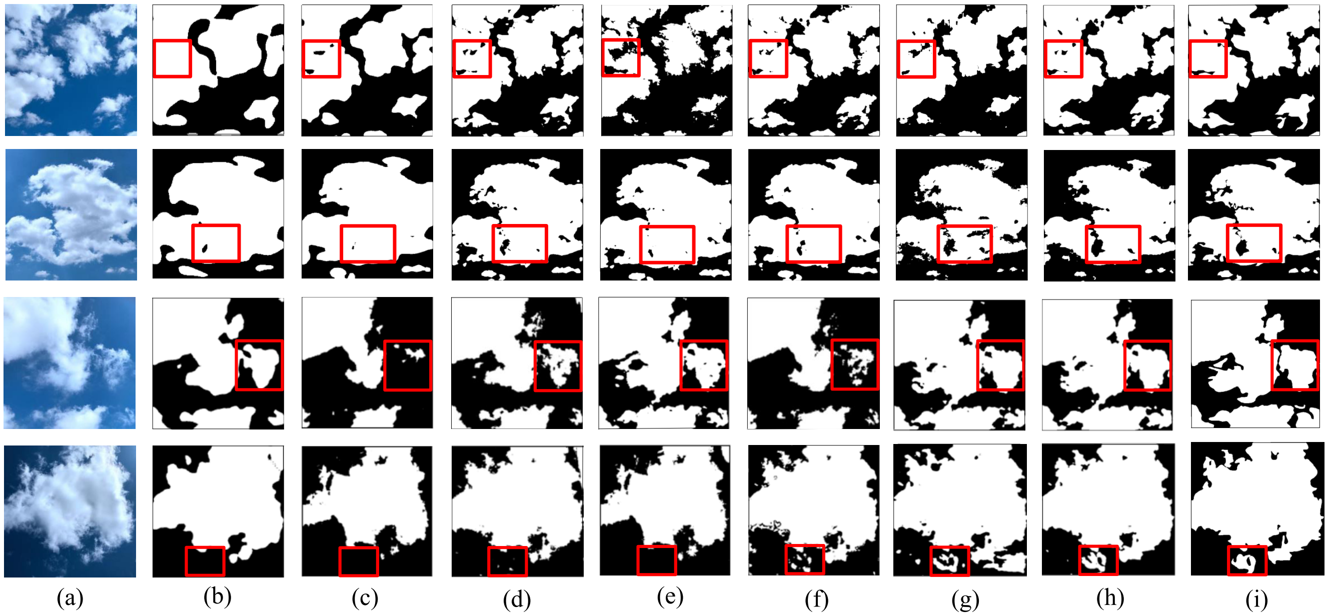

Fig. 5. Predicted cloud masks of different methods: (a) input images, (b) R/B (0.77), (c) Otsu, (d) FCN, (e) U-Net, (f) SegCloud, (g) PSPNet, (h) Ours, and (i) ground-truth cloud masks.

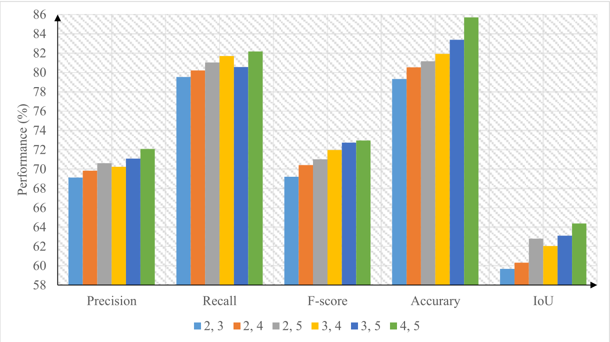

Fig. 6. Detection results with different inputs of DPPM.

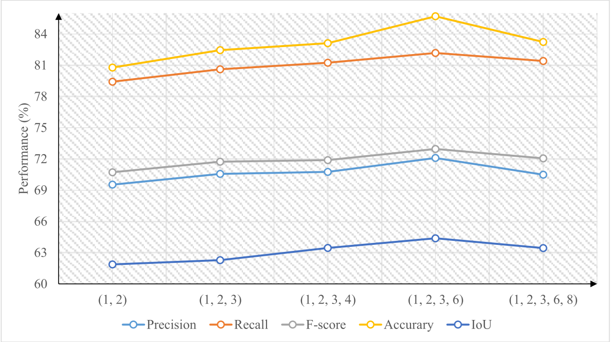

Fig. 7. Detection results with a different number of pyramid levels in DPPM. The numbers in the bracket indicate the number of pyramid levels and the bin sizes of pyramid levels. For example, (1, 2, 3) represents that there are three pyramid levels and the bin sizes of the three pyramid levels are 1 × 1, 2 × 2, and 3 × 3, respectively.

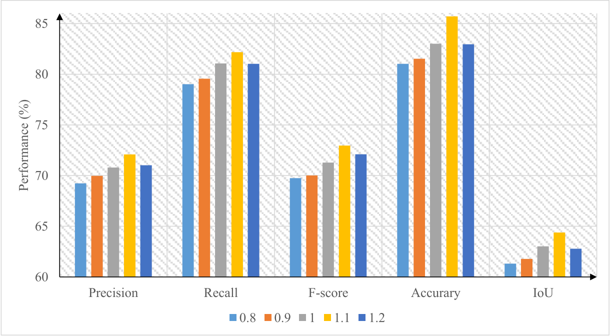

Fig. 8. Detection results with different α's in (10).

In order to intuitively observe the effectiveness of the proposed method, we show the predicted cloud masks of different methods in Fig. 5. From the figure, it can be seen that the detection results of the deep learning methods [see Fig. 5(d)–(h)] are better than those of the threshold-based methods [see Fig. 5(b) and (c)]. The proposed method shows promising performance in the difficult regions, for example, the red rectangles in Fig. 5(b)–(i).

3) Parameter Analysis: In this section, we evaluate the input of DPPM and the influence of the hyperparameters, including the number of pyramid levels in DPPM, the coefficients α in (10), and β in (12).

a) Input of DPPM: In this article, we propose the dual pyramid pooling on the feature maps from two different scales. However, which two scales are selected is important for the detection results. We conduct the experiments with different two scales and the results are shown in Fig. 6. From the figure, we can see that it is reasonable to choose Scale4 and Scale5 as the input of DPPM.

b) Number of pyramid levels in DPPM: The number of pyramid levels in DPPM is related to extract and aggregate the feature maps, and therefore, we conduct experiments with a different number of pyramid levels. The results are shown in Fig. 7 where we can see that when the number of pyramid levels in DPPM is set to 4 and the bin sizes are 1 × 1, 2 × 2, 3 × 3, and 6 × 6, the performance is the best.

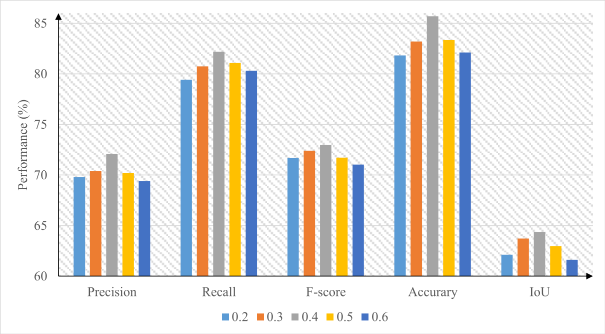

Fig. 9. Detection results with different β's in (12).

c) Coefficient α in (10): The coefficient α is used to balance the two constraints in EDC, and the detection results with different α's are listed in Fig. 8. The detection results increase when α gets larger, while the detection results decrease after 1.1. Hence, we set α to 1.1 in the experiments.

d) Coefficient β in (12): The detection results with different β's are shown in Fig. 9. It can be seen that when β is equal to 0.4, the proposed method achieves the highest detection results.

V. Conclusion

In this article, we have proposed DPNet for ground-based remote sensing cloud detection. Specifically, we first learn the feature maps from different scales using the encoder network, and then, we feed the feature maps of two scales into DPPM that is composed of the dual pyramid pooling and the attention fusion to obtain complete and discriminative features. In order to solve the problem of information loss, we propose EDC to constraint the information of probability maps from the encoder and the decoder. In addition, we release the largest ground-based cloud database TLCDD, which is necessary to promote the research of ground-based remote sensing cloud detection. The experiments on TLCDD have demonstrated the effectiveness of the proposed method.

References

[1] Y. Wang, C. Wang, C. Shi, and B. Xiao, "A selection criterion for the optimal resolution of ground-based remote sensing cloud images for cloud classification," *IEEE Trans. Geosci. Remote Sens.*, vol. 57, no. 3, pp. 4062–4076, Mar. 2019.

[2] C. N. Long, J. M. Sabburg, J. Calbó, and D. Pagés, "Retrieving cloud characteristics from ground-based daytime color all-sky images," *J. Atmos. Ocean. Technol.*, vol. 23, no. 5, pp. 633–652, 2006.

[3] Z. W. Kundzewicz, "Climate change impacts on the hydrological cycle," *Ecohydrol. Hydrobiol.*, vol. 8, nos. 2–4, pp. 195–203, Jan. 2008.

[4] G. Horváth, A. Barta, J. Gál, B. Suhai, and O. Haiman, "Ground-based full-sky imaging polarimetry of rapidly changing skies and its use for polarimetric cloud detection," *Appl. Opt.*, vol. 41, no. 3, pp. 543–559, 2002.

[5] G. Pfister, R. L. McKenzie, J. B. Liley, A. Thomas, B. W. Forgan, and C. N. Long, "Cloud coverage based on all-sky imaging and its impact on surface solar irradiance," *J. Appl. Meteorol.*, vol. 42, no. 10, pp. 1421–1434, 2003.

[6] J. Kalisch and A. Macke, "Estimation of the total cloud cover with high temporal resolution and parametrization of short-term fluctuations of sea surface insolation," *Meteorol. Zeitschrift*, vol. 17, no. 5, pp. 603–611, 2008.

[7] S. Zhenfeng *et al.*, "Cloud detection in remote sensing images based on multiscale features-convolutional neural network," *IEEE Trans. Geosci. Remote Sens.* vol. 57, no. 6, pp. 4062–4076, Jun. 2019.

[8] J. R. Norris, R. J. Allen, A. T. Evan, M. D. Zelinka, C. W. O'Dell, and S. A. Klein, "Evidence for climate change in the satellite cloud record," *Nature*, vol. 536, no. 7614, pp. 72–75, Aug. 2016.

[9] B. Zhong, W. Chen, S. Wu, L. Hu, X. Luo, and Q. Liu, "A cloud detection method based on relationship between objects of cloud and cloud-shadow for Chinese moderate to high resolution satellite imagery," *IEEE J. Sel. Topics Appl. Earth Observ. Remote Sens.*, vol. 10, no. 11, pp. 4898–4908, Nov. 2017.

[10] A. H. Young, K. R. Knapp, A. Inamdar, W. Hankins, and W. B. Rossow, "The international satellite cloud climatology project H-Series climate data record product," *Earth Syst. Sci. Data*, vol. 10, no. 1, pp. 583–593, 2018.

[11] B. Nouri *et al.*, "Determination of cloud transmittance for all sky imager based solar nowcasting," *Sol. Energy*, vol. 181, pp. 251–263, Mar. 2019.

[12] L. Ye, Z. Cao, and Y. Xiao, "DeepCloud: Ground-based cloud image categorization using deep convolutional features," *IEEE Trans. Geosci. Remote Sens.*, vol. 55, no. 10, pp. 5729–5740, Oct. 2017.

[13] C. Shi, Y. Wang, C. Wang, and B. Xiao, "Ground-based cloud detection using graph model built upon superpixels," *IEEE Geosci. Remote Sens. Lett.*, vol. 14, no. 5, pp. 557–567, May 2017.

[14] W. Xie *et al.*, "SegCloud: A novel cloud image segmentation model using a deep convolutional neural network for ground-based all-sky-view camera observation," *Atmos. Meas. Techn.*, vol. 13, no. 4, pp. 1953–1961, Apr. 2020.

[15] E. Baseski and C. Cenaras, "Texture and color based cloud detection," in *Proc. 7th Int. Conf. Recent Adv. Space Technol. (RAST)*, Jun. 2015, pp. 311–315.

[16] D. Tulpan, C. Bouchard, K. Ellis, and C. Minwalla, "Detection of clouds in sky/cloud and aerial images using moment based texture segmentation," in *Proc. Int. Conf. Unmanned Aircr. Syst. (ICUAS)*, Jun. 2017, pp. 1124–1133.

[17] J. Dai, K. He, and J. Sun, "Convolutional feature masking for joint object and stuff segmentation," in *Proc. IEEE Conf. Comput. Vis. Pattern Recognit. (CVPR)*, Jun. 2015, pp. 3992–4000.

[18] S. Dev, A. Nautiyal, Y. H. Lee, and S. Winkler, "CloudSegNet: A deep network for nychthemeron cloud image segmentation," *IEEE Geosci. Remote Sens. Lett.*, vol. 16, no. 12, pp. 1814–1818, Dec. 2019.

[19] J. Yang, J. Guo, H. Yue, Z. Liu, H. Hu, and K. Li, "CDNet: CNN-based cloud detection for remote sensing imagery," *IEEE Trans. Geosci. Remote Sens.*, vol. 57, no. 8, pp. 6195–6211, Aug. 2019.

[20] S. Liu, L. Duan, Z. Zhang, X. Cao, and T. S. Durrani, "Ground-based remote sensing cloud classification via context graph attention network," *IEEE Trans. Geosci. Remote Sens.*, vol. 60, pp. 1–11, 2022, doi: 10.1109/TGRS.2021.3063255.

[21] S. Dev, Y. H. Lee, and S. Winkler, "Color-based segmentation of sky/cloud images from ground-based cameras," *IEEE J. Sel. Topics Appl. Earth Observ. Remote Sens.*, vol. 10, no. 1, pp. 231–242, Jan. 2016.

[22] T. Fa, W. Xie, Y. Wang, and Y. Xia, "Development of an all-sky imaging system for cloud cover assessment," *Appl. Opt.*, vol. 58, no. 20, pp. 5516–5524, Jul. 2019.

[23] O. Ronneberger, P. Fischer, and T. Brox, "U-Net: Convolutional networks for biomedical image segmentation," in *Proc. Med. Image Comput. Comput.-Assist. Intervent*, 2015, pp. 234–241.

[24] A. Kreuter, M. Zangerl, M. Schwarzmann, and M. Blumthaler, "All-sky imaging: A simple, versatile system for atmospheric research," *Change*, vol. 48, no. 6, pp. 1017–1091, 2009.

[25] M. Souzaecher, E. Pereira, L. Bins, and M. Andrade, "A simple method for the assessment of the cloud cover state in highlatitude regions by a ground-based digital camera," *J. Atmos. Ocean. Technol.*, vol. 23, no. 3, pp. 427–447, 2006.

[26] J. Yang, W. Lu, Y. Ma, and W. Yao, "An automatic ground-based cloud detection method based on adaptive threshold," *J. Appl. Meteorol. Sci.*, vol. 20, no. 6, pp. 713–721, Sep. 2009.

[27] S. Liu, L. Zhang, Z. Zhang, C. Wang, and B. Xiao, "Automatic cloud detection for all-sky images using superpixel segmentation," *IEEE Geosci. Remote Sens. Lett.*, vol. 12, no. 2, pp. 354–358, Feb. 2015.

[28] H. Zhao, J. Shi, and X. Qi, "Pyramid scene parsing network," in *Proc. IEEE Conf. Comput. Vis. Pattern Recognit.*, Jul. 2017, pp. 2881–2890.

[29] M. Mostajabi, P. Yadollahpour, and G. Shakhnarovich, "Feedforward semantic segmentation with zoom-out features," in *Proc. IEEE Conf. Comput. Vis. Pattern Recognit. (CVPR)*, Jun. 2015, pp. 3376–3385.

[30] Z. Zhang, S. Yang, S. Liu, B. Xiao, and X. Cao, "Ground-based cloud detection using multiscale attention convolutional neural network," *IEEE Geosci. Remote Sens. Lett.*, vol. 19, pp. 1–5, 2022, doi: 10.1109/LGRS.2021.3106337.

[31] Z. Qiao, Y. Zhou, D. Yang, Y. Zhou, and W. Wang, "SEED: Semantics enhanced encoder-decoder framework for scene text recognition," in *Proc. IEEE/CVF Conf. Comput. Vis. Pattern Recognit. (CVPR)*, Jun. 2020, pp. 13528–13537.

[32] J. Yao, S. Fidler, and R. Urtasun, "Describing the scene as a whole: Joint object detection, scene classification and semantic segmentation," in *Proc. IEEE Conf. Comput. Vis. Pattern Recognit.*, Jun. 2012, pp. 702–709.

[33] K. Yuan, G. Meng, D. Cheng, J. Bai, S. Xiang, and C. Pan, "Efficient cloud detection in remote sensing images using edge-aware segmentation network and easy-to-hard training strategy," in *Proc. IEEE Int. Conf. Image Process. (ICIP)*, Sep. 2017, pp. 61–65.

[34] X. Hou *et al.*, "Dual adaptive pyramid network for cross-stain histopathology image segmentation," in *Proc. Int. Conf. Med. Image Comput. Computer-Assisted Intervent*, vol. 2019, pp. 101–109.

[35] D. O'Neill, B. Xue, and M. Zhang, "Evolutionary neural architecture search for high-dimensional skip-connection structures on DenseNet style networks," *IEEE Trans. Evol. Comput.*, vol. 25, no. 6, pp. 1118–1132, Dec. 2021, doi: 10.1109/TEVC.2021.3083315.

[36] X. J. Mao, C. Shen, and Y. B. Yang, "Image restoration using very deep convolutional encoder-decoder networks with symmetric skip connections," in *Proc. Adv. Neural Inf. Process. Syst.*, 2016, pp. 2802–2810.

[37] J. Long, E. Shelhamer, and T. Darrell, "Fully convolutional networks for semantic segmentation," in *Proc. IEEE Conf. Comput. Vis. Pattern Recognit. (CVPR)*, Jun. 2015, pp. 3431–3440.

[38] M. Zhai, X. Xiang, R. Zhang, N. Lv, and A. El Saddik, "Optical flow estimation using dual self-attention pyramid networks," *IEEE Trans. Circuits Syst. Video Technol.*, vol. 30, no. 10, pp. 3663–3674, Oct. 2020.

[39] K. He, X. Zhang, S. Ren, and J. Sun, "Deep residual learning for image recognition," in *Proc. IEEE Conf. Comput. Vis. Pattern Recognit. (CVPR)*, Jun. 2016, pp. 770–778.

[40] K. He, X. Zhang, S. Ren, and J. Sun, "Spatial pyramid pooling in deep convolutional networks for visual recognition," *IEEE Trans. Pattern Anal. Mach. Intell.*, vol. 37, no. 9, pp. 1904–1916, Jul. 2015.

[41] R.-G. Zhou, H. Yu, Y. Cheng, and F.-X. Li, "Quantum image edge extraction based on improved Prewitt operator," *Quantum Inf. Process.*, vol. 18, no. 9, pp. 1–24, Sep. 2019.

Zhong Zhang (Senior Member, IEEE) received the Ph.D. degree from the Institute of Automation, Chinese Academy of Sciences, Beijing, China.

He is currently a Professor with Tianjin Normal University, Tianjin, China. He has published about 110 papers in international journals and conferences, such as the IEEE TRANSACTIONS ON GEOSCIENCE AND REMOTE SENSING, IEEE TRANSACTIONS ON FUZZY SYSTEMS, *Pattern Recognition*, IEEE TRANSACTIONS ON CIRCUITS SYSTEMS FOR VIDEO TECHNOLOGY, IEEE TRANSACTIONS ON INFORMATION FORENSICS AND SECURITY, *Signal Processing* (Elsevier), IEEE Conference on Computer Vision and Pattern Recognition (CVPR), Association for the Advance of Artificial Intelligence (AAAI) Conference on Artificial Intelligence, International Conference on Pattern Recognition (ICPR), and International Conference on Image Processing (ICIP). His research interests include remote sensing, computer vision, and deep learning.

Shuzhen Yang is currently pursuing the master's degree with Tianjin Normal University, Tianjin, China.

Her research interests include ground-based cloud analysis and deep learning.

Shuang Liu (Senior Member, IEEE) received the Ph.D. degree from the Institute of Automation, Chinese Academy of Sciences, Beijing, China, in 2014.

She is currently a Professor with Tianjin Normal University, Tianjin, China. She has published over 60 papers in major international journals and conferences. Her research interests include computer vision, remote sensing, and deep learning.

Xiaozhong Cao received the Ph.D. degree in automatic control theory and application from the Institute of Automation, Chinese Academy of Sciences, Beijing, China, in 1996.

He is currently a Professor with the Meteorological Observation Centre, China Meteorological Administration, Beijing. His research interests include the theory of meteorological observation and climate change, and automatic meteorological observation.

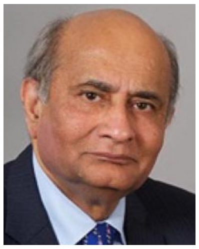

Tariq S. Durrani (Life Fellow, IEEE) is currently a Research Professor with the University of Strathclyde, Glasgow, U.K. He has authored 350 publications and supervised 45 Ph.D. students. His research interests include artificial intelligence (AI), signal processing, and technology management.

Prof. Durrani is a fellow of the U.K. Royal Academy of Engineering, the Royal Society of Edinburgh, Institution of Engineering and Technology (IET), and the Third World Academy of Sciences. He was elected as a Foreign Member of the Chinese Academy of Sciences and the U.S. National Academy of Engineering in 2021 and 2018, respectively.